Structural Evaluation of Carbon and Stainless Steel Plates with Staggered Bolts Subjected to Tension Forces

J. de J. Santos[1], P. C. G. S. Vellasco[2], L. R. O. Lima[2], S. A. L. Andrade[1], A. T. Silva[3] & J. G. S. Silva[2]

[1]Pontifical Catholic University of Rio de Janeiro, [2]State University of Rio de Janeiro, [3]State University of Rio de Janeiro

Abstract

The present investigation presents experimental and numerical studies aiming to evaluate the tension capacity of stainless and carbon steel bolted structural elements performed over the last few years. In this problem the net section rupture represents one of the controlling ultimate limit states usually verified for structural elements submitted to tension normal stress and is the focus of the present investigation. The obtained results are discussed and compared in terms of the stress distribution and force-displacement curves, among others. The assessment of the results was made by comparisons to the Eurocode 3 provisions for carbon and stainless steels. It is also interesting to observe that the Eurocode 3, part 1.4, used for stainless steel structural design is still largely based in analogies to carbon steel structural behaviour. In the present investigation large strains were observed in the stainless plates indicating that the current design criteria based on deformation limits need to be re-evaluated. This was especially due to the differences in the yield to ultimate deformation and stress ratios observed when the carbon or stainless specimens are considered.

Keywords

steel structural, beam-to-column joints, extended endplate joints, semi-rigid joints, experimental analysis, component method

1 Introduction

The development of the construction process and, the new tendencies adopted in the architecture design conception, highlighted the need for materials that can combine versatility with durability. On the other hand stainless steel present itself as a promising material for constructions that require these characteristics, mainly related to high corrosion strength avoiding the need for short period maintenance. Stainless steel is indicated, as a structural element in construction form multiple reasons. Its high ductility allows its use in structures subjected to cyclic loadings, enabling the dissipation of the energy associated to this type of loads, through load redistributions before the structural collapse. The cost reduction achieved with the less need for structure maintenance, and the increase in its capacity to dissipate impact loads, also enhanced the stainless steel structure reliability.

Changes of attitudes associated to the building construction industry and a global transition for a sustainability development reduction in environmental impacts has been causing an increase in the stainless steel use. Despite these facts, Current stainless steel design codes like the Eurocode 3, part 1.4 [3], are still largely based in carbon steel structural analogies [2]. This strategy was used as a first attempt to produce specific stainless steel structural design rules, enabling engineers to perform a smooth transition for the stainless steel design.

The search for a broader understanding of the actual behaviour of stainless steel bolted joint has motivated several investigations to be performed in various research centres like: Burgan et al. [4], Kouhi et al. [5], Van Den Berg [6], Gardner and Nethercot [7]. The main motivation for these studies was the search for the most cost-effective structure resulting from an optimum joint design, as well as an improvement of the joint fabrication and assembly costs. The complete understanding of the stainless steel bolted joints response will also conduct to the production of more accurate design equations that will probably be incorporated in the future editions of the stainless steel design standards.

A study of the bearing collapse of austenitic and ferritic stainless steel joints, in single and double shear, with thin and thick plate, as illustrated in Figure 1, was made by Salih et al. [8] focusing on the variables e_1/d_0 and e_2/d_0. The authors evaluated the equivalent strain percentages that can happen in various angles of the bolt holes and plate arrangements. The stainless steel stress *versus* strain curves is different from the carbon steel stress vs. strain curves presenting a higher ultimate stress capacity and a nonlinear relationship. These differences pointed for a better assessment of the carbon steel design rules to be adapted to a consistent stainless steel design.

Paper Presented by Prof. Pedro Vellasco - pvellasco@globo.com

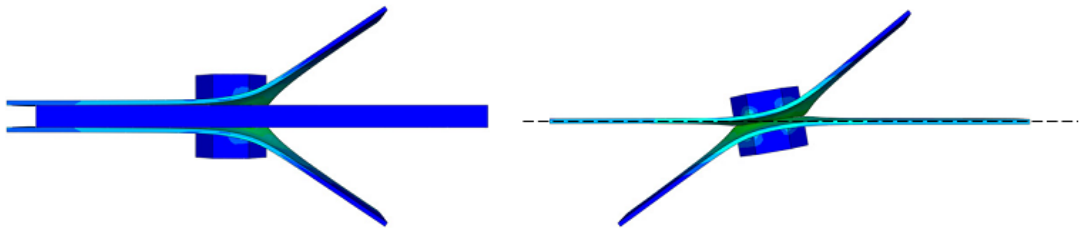

Figure 1 Numerical tests [8]

Experimental studies indicated that different types of collapses, especially due to serviceability limitations, were observed in stainless steel joints with thin and thick plates under shear. Numerical studies also pointed out that the stainless steel ultimate stress f_u could be adopted, instead of the reduced stainless steel ultimate stress $f_{u,red}$, proposed by the Eurocode in the joint shear design formulae. The net section rupture represents one of the ultimate limit states usually verified for structural elements submitted to tension normal stress. The present chapter presents an experimental numerical investigations aiming to evaluate the tension capacity of carbon and stainless steel bolted structural elements. The results are discussed and compared in terms of the stress distribution (that detects, for instance, first yield), and force-displacement curves, among others. The assessment of the results was made by comparisons to the Eurocode 3 provisions for carbon and stainless steels. The investigation indicated that when stainless steel is used in certain structural engineering applications like joints under shear forces, the current design criteria based on deformation limits need to be re-evaluated specially due to the differences in the yield to ultimate deformation and stress ratios.

2 Eurocode 3 Provisions

The current investigation uses the European design code for stainless steel elements - Eurocode 3, part 1.4 [3]. In this design standard, the failure modes for a plate with holes under tension axial forces are governed by two ultimate limit states: the gross area yield and the net area tension rupture. The presence of staggered holes in the transversal section, Figure 2, difficult an immediate identification of the plate critical net section. This process is not new since in 1922, Crochrane [9], performed one of the first attempts to characterize staggered bolted connection failure modes by the use of eq. (1). This expression adds a term to the original net width to obtain the final net section area and is present in major steel design codes all over the world.

$$b_n = b - d_b + \frac{s^2}{4p} \qquad (1)$$

In the previous equation b is the plate width, d_b is the bolt diameter, s and p represent the staggered centre to centre hole distances measured parallel and perpendicular to the member axis. The Eurocode 3, part 1.4 (2003) [3], establishes the guidelines for the stainless steel plate design submitted to axial tension forces. The structure failure is associated to the smallest tension axial force obtained considering two limit states: gross cross-section plastic resistance given by eq. (2), or the ultimate net cross-section tension rupture expressed by eq. (3).

$$N_{pl,Rd} = \frac{A_g \cdot f_y}{\gamma_{M0}} \qquad (2)$$

where $N_{pl,Rd}$ is the tension design plastic resistance,

A_g is the plate gross area,

f_y is the steel yielding stress,

γ_{M0} is the partial safety factor, in this case equal to 1.

$$N_{u,Rd} = \frac{k_r \cdot A_n \cdot f_u}{\gamma_{M2}} \qquad \text{with} \qquad k_r = \left(1 + 3r\left(d_0 / u - 0.3\right)\right) \qquad (3)$$

where A_n is the net cross-section plate area,

f_u is the steel tension rupture stress,

k_r is obtained from eq. (4),

γ_{M2} is the partial safety factor, in this case equal to 1.25,

r is the ratio between the number of bolts at the cross-section and the total joint bolt number,

d_0 is the hole diameter,

$u = 2.e_2$ but $u \leq p_2$ where e_2 is the edge distance measured from the bolt hole centre to its adjacent edge, in the direction perpendicular to the load transfer direction and p_2 is the hole centre-to-centre distance measured perpendicular to the load axis.

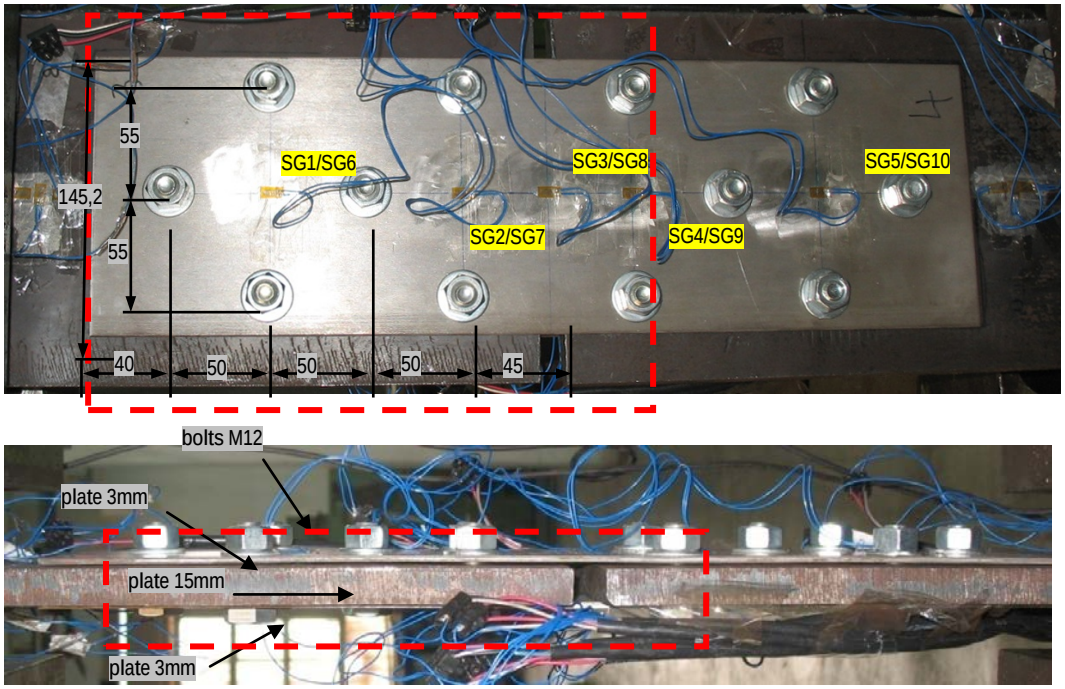

Figure 2 Cover plate joint detail and strain gauges location.

The tension joint design has also some additional recommendations:

- in bolted joints, the hole width should be considered 2 mm larger than the nominal bolt diameter, perpendicular to the applied force direction;
- in the case of staggered holes, when a diagonal direction to the load axis or zigzag is considered, the net width should be calculated first deducing from the initial gross width, all the holes present in it, and after that adding for each staggered holes a value equal to $s^2/4p$, where s and g, represent the considered longitudinal and traverse hole spacing;
- the bolted joint critical net width is the smallest evaluated net width for all the different net rupture possibilities;
- for angles, the dimension *p* of opposite legs holes is equal to the sum of the dimensions, measured from the angle corner, minus its thickness;
- the net cross-section area for joints with fillet or spot welds present in the holes should not consider the weld metal area;
- joints without holes should be evaluated considering that the net area is equal to the gross area, $A_{net} = A_g$.

3 Experimental Investigations

Kim and Kuwamura [10] performed a series of experiments on austenitic stainless steel SUS304, bolted joints and compared their results with bi and three-dimensional finite element models using contact elements, Figure 3.

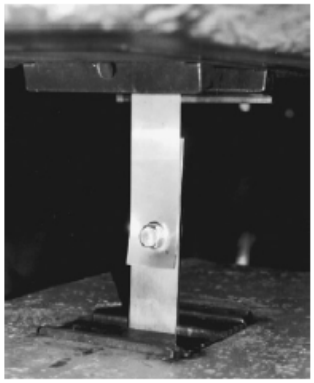

Figure 3: Kim and Kuwamura experiments [10].

The experimental programme performed by Kim and Kuwamura [10] involved three different bolt layout configurations, as illustrated in Figure 4. The single plane shear experiments were made on Austenitic stainless steel SUS304 plates with 1.5 mm and 3 mm thicknesses and 12mm bolts (A2-50 SUS bolts and 10T-SUS HFSG bolts). The plate specimen ends were attached to an Amsler universal test machine that gradually applied the load to the tested plates.

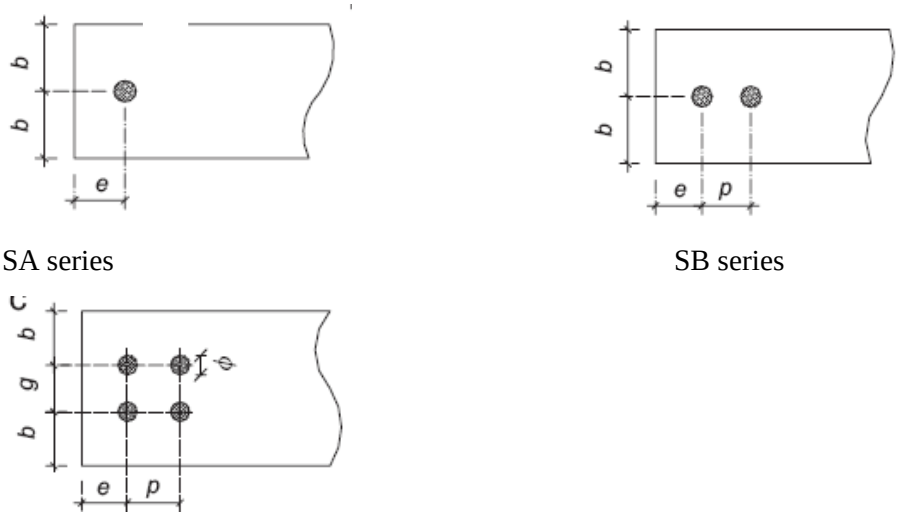

SA series SB series

SC series

Figure 4 Kim and Kuwamura joint layouts [10].

The experimental results can be depicted in Table 1, with their respective dimensions for each tests and its associated failure mode. The true stress vs. true strain curve obtained using the equations (8) and (9), respectively where σ_t , ε_t , f_y ,and ,ε_n represent the true stress, the true strain the yield stress and original measured strain, respectively.

Table 1 Summary of experimental results [10]

Series	Specimen	Thickness (mm)	e (mm)	b (mm)	g (mm)	p (mm)	Failure mode	Ultimate load (kN)
SA (1 hole)	SA1-1	1.5	12	25	-	-	B	12.28
	SA2-2	3.0	18	25	-	-	B	48.05
SB (2 holes)	SB1-4	1.5	60	25	-	30	A	43.34
	SB2-4	3.0	60	25	-	30	A	85.62
SC (3 holes)	SC1-4	1.5	60	55	30	30	C	79.53
	SC2-1	3.0	12	55	30	30	B-C	115.62
	SC2-3	3.0	30	55	30	30	C	162.34
	SC2-4	3.0	60	55	30	30	C	163.30

$$\sigma_t = f_y(1+\varepsilon_n) \quad (8)$$

$$\varepsilon_t = ln(1+\varepsilon_n) \quad (9)$$

An innovative experimental program was used to evaluate the tension capacity of carbon and stainless steel plates with staggered bolts [11]. The first series of experiments experiments involved bolted cover plate joints made of stainless steel A304 and carbon steel USI300 denominated EX_INOX_Y and EX_CARBON_Y [11], respectively. All the geometrical properties for the tests are presented in Table 2. The bolted joints were made of two 3 mm thick stainless and carbon steel plates and two 15 mm thick carbon steel plates used to transfer load to the 3mm plate with a 5 mm gap. The horizontal bolt pitch, s, was modified in each test and the vertical bolt pitch, p, were 55 mm (see Figure 5). The bolted cover plate joint tests were carried out on a 600kN Universal Lousenhausen test machine, see Figure 5. The data acquisition in terms of strains, displacements and applied load was performed using the National Instruments system

NI-PXI-1050. The strains measurements were performed using linear strain gauges located in both stainless steel plates named SG, Figure 2.

Table 2 Summary of the first series of experimental tests [11].

ID	s (mm)	p (mm)	e1 (mm)	e2 (mm)	d0 (mm)	STEEL	t_{base} (mm)	bolts
E3_CARB_S50	50	55	40	17.6	14.7	carbon	15	6
E4_CARB_S30	30	55	40	17.6	14.7	carbon	15	6
E5_STAIN_S50	50	55	40	17.6	14.7	stainless	15	6
E6_CARB_S30_P10	30	55	40	17.6	14.7	carbon	10	6
E7_STAIN_S30	30	55	40	17.6	14.7	stainless	15	6
E8_CARB_S50_P8	50	55	40	17.6	14.7	carbon	8	6
E9_STAIN_S23	23	55	40	17.6	14.7	stainless	15	6

a) Universal test machine, 600kN

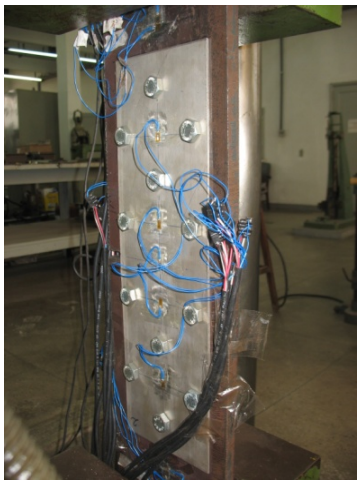

b) cover plate joint detail

Figure 5 Santos et al test layout [11].

The tensile coupons test curves presented a nonlinear expected behaviour, mainly for the stainless steel – see Figure 6. The stainless steel yield stress was determined using a straight line parallel to the initial stiffness at a 0.2% deformation, leading to a value equal to 350.6 MPa while the ultimate tension stress was 710.7 MPa. For the carbon steel, these values were equal to 386.8 MPa and 478.7 MPa for the yield and ultimate stress, respectively. These results are summarised on Table 3. Figure 6 also present the results of a true stress *versus* true strain curve obtained using the equations (8) and (9), respectively. This curve was used in the finite element modelling due to the large strain and stresses associated to the investigated problem.

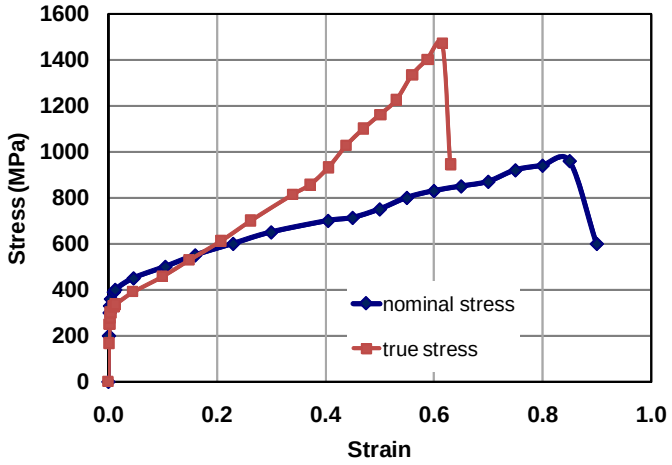

Figure 6 Stress *versus* strain curves for the stainless steel A304.

Table 3 Summary of tensile coupons tests [11].

Carbon coupons	f_y (MPa)	f_u (MPa)	Stainless coupons	f_y (MPa)	f_u (MPa)
AC 1	388.97	485.97	I 1	352.30	713.10
AC 2	383.77	478.43	I 2	345.70	699.00
AC 3	348.29	450.55	I 3	352.20	730.50
AC 4	404.39	495.91	I 4	347.80	692.80
AC 5	401.31	488.81	I 5	349.60	725.80
AC 6	394.01	472.43	I 6	356.10	703.10
Mean	386.79	478.68	Mean	350.62	710.72
Standard Deviation	20.34	16.02	Standard Deviation	3.70	15.11

Figure 7 presents the comparison between the results from tests E3_CARB_S50 and E5_STAIN_S50 in terms of the load *versus* axial displacement curves. In this figure, it may be depicted out the experimental ultimate loads of 310.0 kN and 469.4 kN for E3_CARB_S50 and E5_STAIN_S50 tests, respectively. According to the Eurocode 3 [2], [3], eq. (2) and (3), for the E3_CARB_S50 test, the design resistances were 337.0 kN for gross cross-section plastic resistance and 298.7 kN for ultimate net cross-section tension rupture (section with three holes). While for the E5_STAIN_S50 test, these values were 305.5 kN and 810.8 kN (net section with three holes), respectively. The partial safety factor was taken equal to 1.0. Figure 7 also indicates that in both tests, the test rupture occurred in the section represented by two holes near to joint symmetry axis. Despite the fact that, for the carbon steel test E3_CARB_S50, the theoretical and experimental values presented a good agreement, the stainless steel test E5_STAIN_S50 presented a larger difference in terms of the ultimate design equation and test loads.

Figure 8 presents the comparison between the results from tests E4_CARB_S30 and E7_STAIN_S30 in terms of the load *versus* displacement curves. In this figure, it may be depicted the experimental ultimate loads of 303.6 kN and 545.8 kN for E4_CARB_S30 and E7_STAIN_S30 tests, respectively. According to the Eurocode 3 [2], [3], eq. (2) and (3), for the E4_CARB_S30 test, the design resistances were 337.0 kN for gross cross-section plastic resistance and 291.7 kN for ultimate net cross-section tension rupture (section with three holes). In the case of the E5_STAIN_S50 test, these values were 305.5 kN and 791.9 kN (net section with three holes), respectively. Figure 8 indicates that in both tests, the rupture occurred in the section represented by two holes near to joint symmetry axis. One more time the carbon steel test E3_CARB_S50 theoretical and experimental values presented a good agreement while the stainless steel test E5_STAIN_S50, still shown a non-negligible difference of the ultimate design equation and test loads.

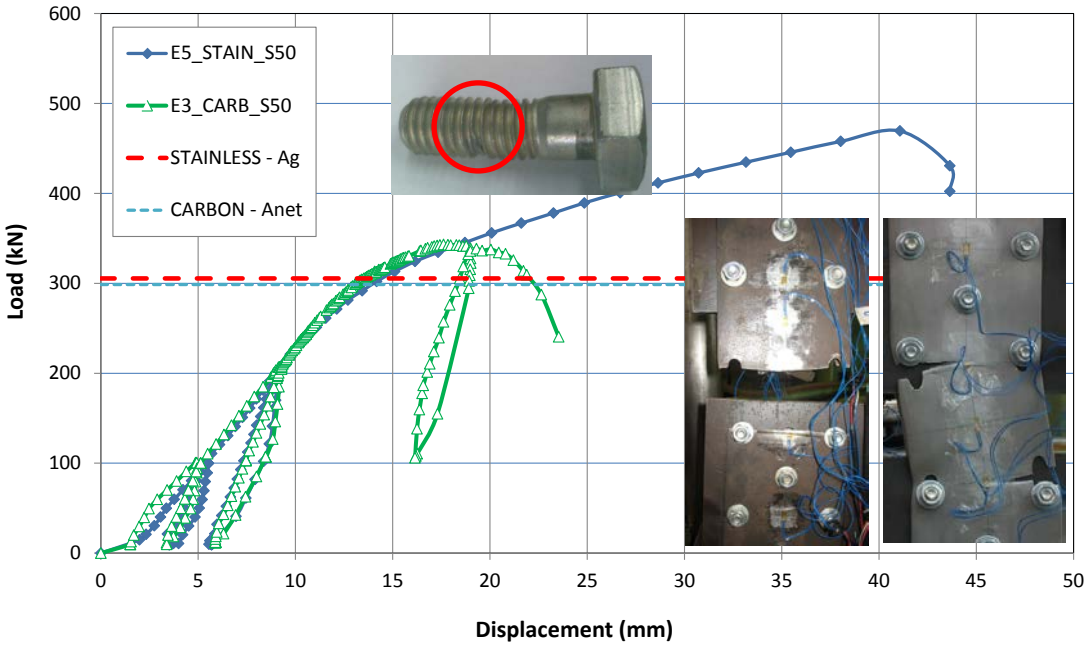

Figure 7 Load *versus* displacement - E3_CARBON_S50 & E5_STAIN_S50 [11].

Considering the difference between the failure modes for the two stainless steel joints presented before, a third test, E9_STAIN_S23, was performed to investigate this issue where the horizontal bolt pitch was taken equal to 23mm. This value was considered increase the difference between the load failure in sections with two and three bolts, respectively. According to Eurocode 3 [2], [3], for this test, the design resistances were 305.4 kN for gross cross-section plastic resistance and 787.7 kN for ultimate net cross-section tension rupture (section with three holes). Figure 9 presents the load *versus* displacement for this test where the ultimate experimental load was equal to 526.5 kN. It can also be observed that the joint rupture occurred in the net section passing through three bolts, in agreement with the Eurocode 3 provision [2], [3]. Despite this fact, the design equation and the experimental ultimate loads still presented a large difference.

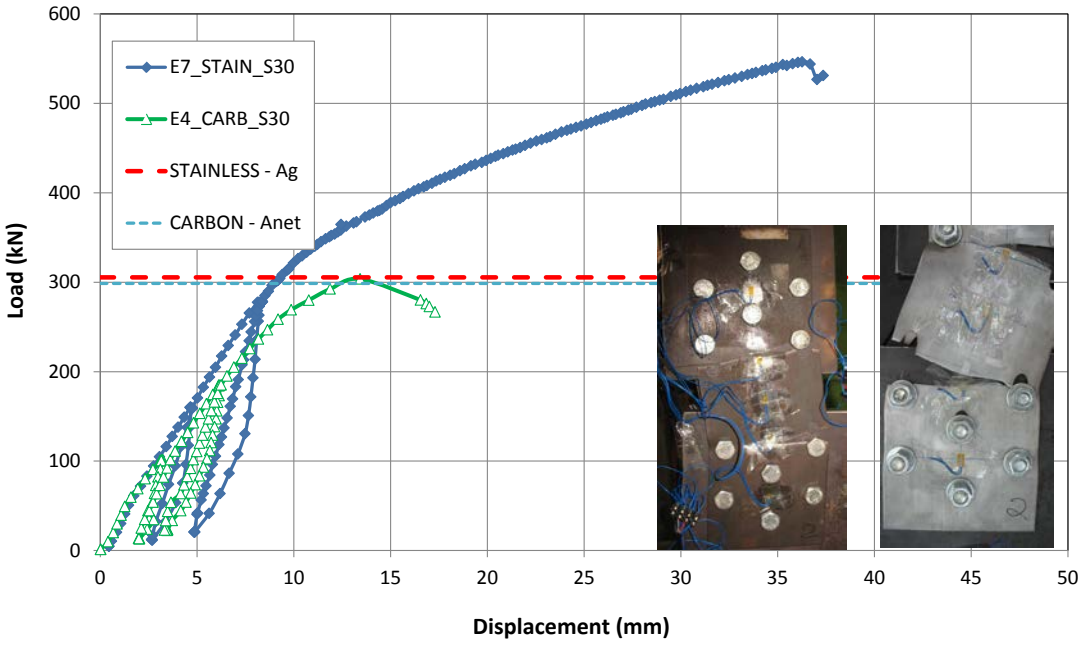

Figure 8 Load *versus* displacement - E4_CARBON_S30 & E7_STAIN_S30 [11].

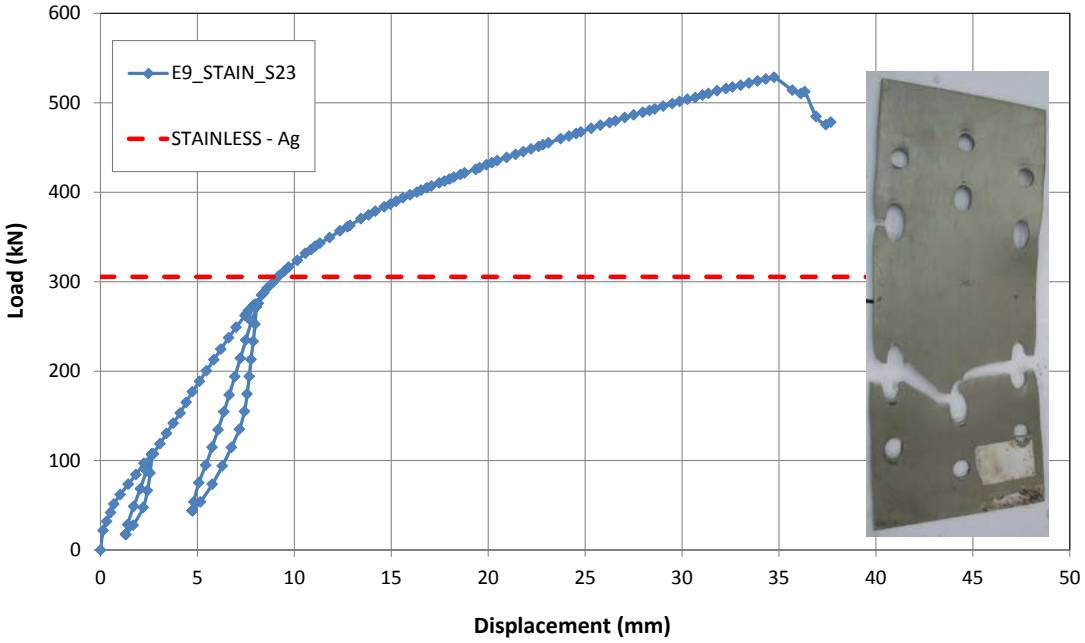

Figure 9 Load *versus* displacement - E9_STAIN_S23 [11].

A summary of these results is presented in Table 4. It may be concluded that for carbon steel joints, a good agreement was observed comparing the theoretical and experimental results. Alternatively, for the stainless steel joints, larger differences were found in terms of ultimate (rupture) loads.

Table 4 Summary of experimental tests [11].

ID	Experiment Failure Mode	Experiment Ultimate Load (kN)	EC3 Failure Mode	EC3 Ultimate Load (kN)	% $\frac{EXP}{EC3}$
E3_CARB_S50	2H	310.0	3H	298.3	3.9
E4_CARB_S30	2H	296.0	3H	282.5	4.8
E5_INOX_S50	2H	480.0	AB	302.9	58.5
E6_CARB_S30_P10	3H	309.5	3H	282.5	9.6
E7_INOX_S30	2H	459.0	AB	302.9	51.5
E8_CARB_S50_P8	2H	326.0	2H	282.5	13.3
E9_INOX_S23	3H	436.0	AB	302.9	43.9
2H: two hole net rupture; 3H: three hole net rupture and AB: gross section yielding					

Another key issue was also studied in the current study and involved the assessment of the influence of the load application plate thickness, adopted initially equal to 15mm (E3_CARB_S50 and E4_CARB_S30). Two other tests were performed, E6_CARB_S30_P10 (load plate thickness equal to 10 mm) and E8_CARB_S50_P8 (load plate thickness equal to 8 mm). Comparing the E3, E8 and E4 tests with E6, Figure 10, it may be concluded that the load application plate thickness significantly alters the joint response in terms of ultimate load and associated failure mode.

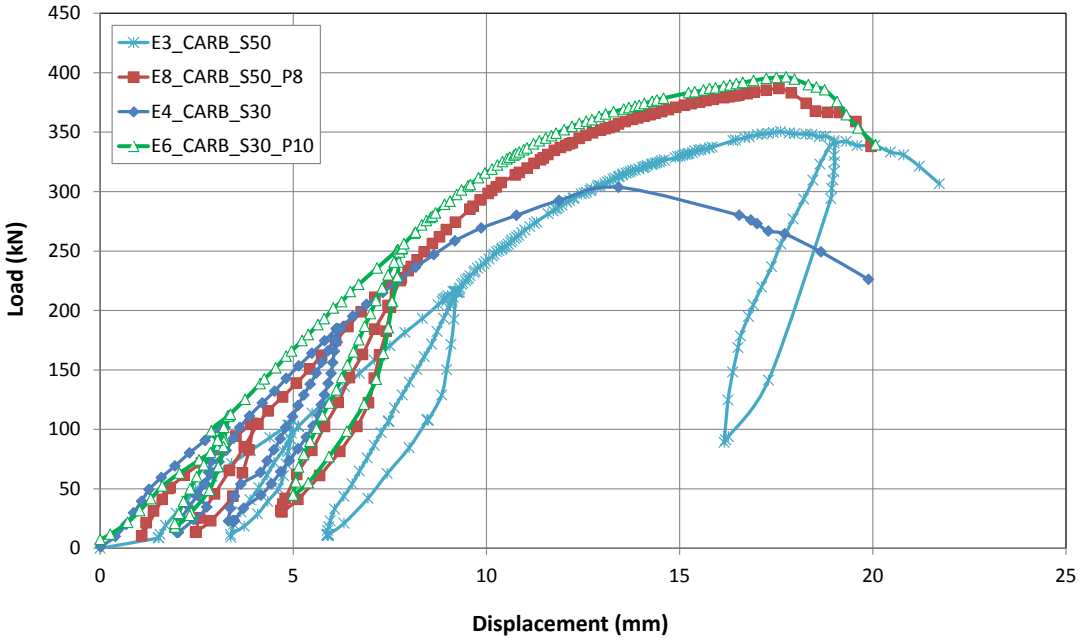

Figure 10: Load *versus* displacement – load plate thickness variation [11].

The second series of experiments further investigated the influence of the load application plate thickness. Three different layouts of the model geometry were investigated using the application plate model with a 6mm thickness equal to the sum of the external tested plates as can be observed in Figure 11 and in Table 5. One plate was also tested with bolts in a single row to verify the possibility of collapse associated to the yield of the plate gross section. In addition to the original plate layout a second configuration was tested reducing the g, bolt vertical spacing from 55mm to 36 mm.

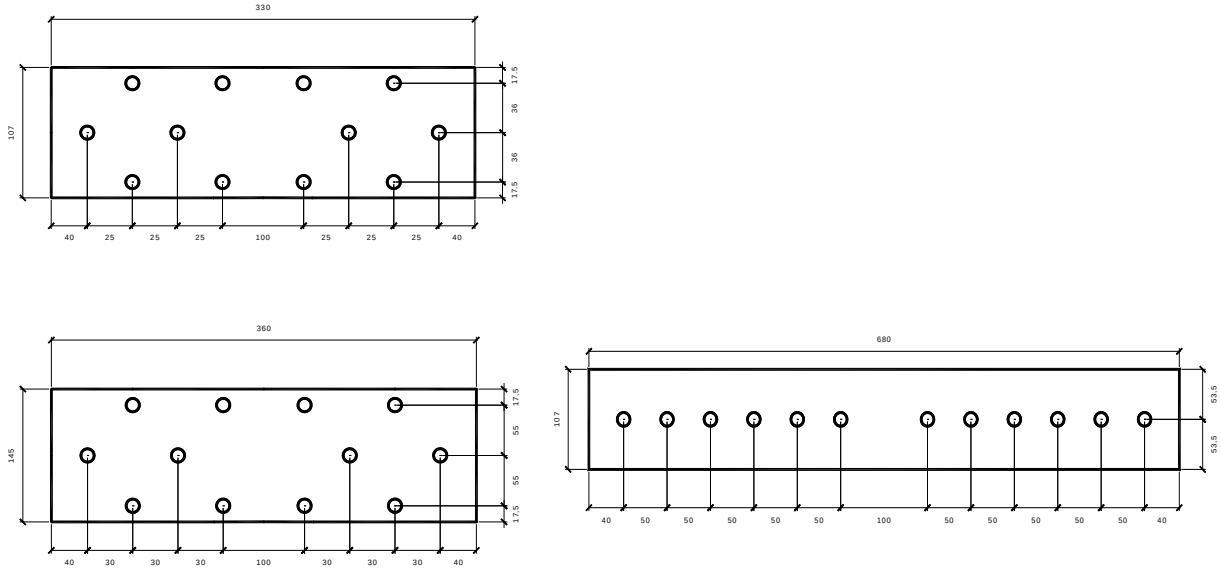

Figure 11 Second series of experiments geometry layout.

Table 5 Second series of experiments geometry.

Test	L (mm)	s (mm)	g (mm)	t (mm)	Load (kN)	Displacement (mm)	Test Failure Mode
AC_145_55_30	145	30	55	6	300.15	18.60	2H
AC_145_55_25	145	30	55	6	314.25	17.61	3H
AC_107_36_30	107	25	36	6	221.65	16.37	2h
AC_107_36_25	107	25	36	6	214.00	16.01	3H

AC_107_ 0 50	107	50	0	6	260.30	21.26	1H

The second series of test results are depicted in Figure 12 and Figure 13. These tests confirmed the influence of the internal plate thickness over the plate failure mode and serve as means to determine the limits between the plate net rupture passing through two or three holes (i.e. s, bolt horizontal spacing between 25 mm & 30 mm), These test are continuing with an s bolt horizontal spacing equal to 28 mm to further delimit these two failure modes. A clear distinction of behaviour is also observed between the test with the single bolt row layout and the others.

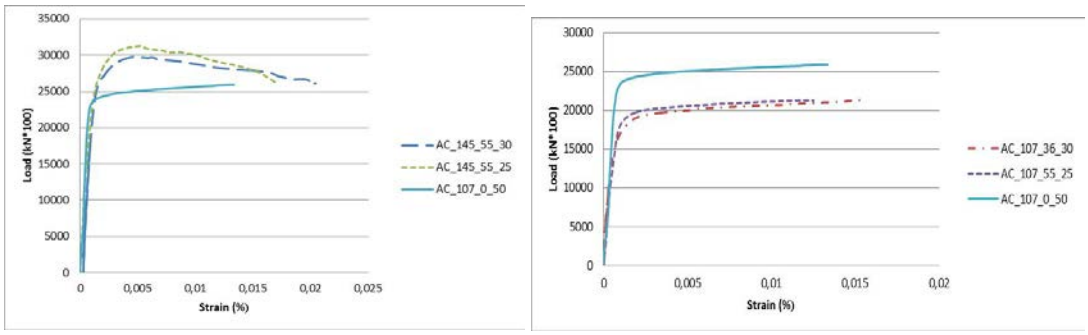

Figure 12 Load *versus* strain curves for the second series of experiments.

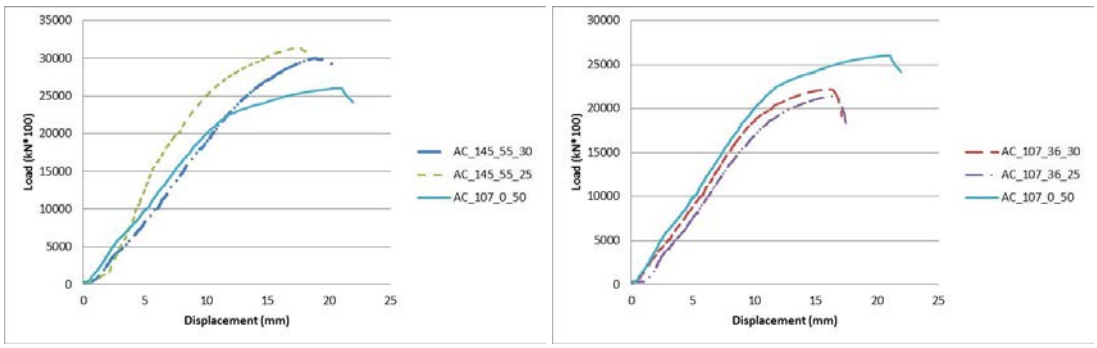

Figure 13 Load *versus* displacement curves for the second series of experiments.

4 Numerical Investigations

Finite Element numerical analyses provide a relatively inexpensive and time efficient alternative to physical experiments. Despite this fact, due to their nature these numerical simulations [12] have to be properly calibrated against experimental test results. If the validity of FE analysis is assured, it is possible to investigate the structural behaviour against a wide range of parameters with the FE model [13].

A finite element model was used to investigate the tension capacity of cover plate joints was developed with the aid of the Ansys 11 FE package [14]. The numerical model adopted solid elements (SOLID45) defined by eight nodes with three degrees of freedom per node: translations in the nodal x, y and z directions. The adopted mesh was chosen so that the elements had a proportion and size to avoid numerical problems.

Contact elements (CONTA174 and TARGE170) presented in the Ansys Elements Library [14] were considered between the plates and between the holes and the bolt shanks. The load was applied by means of axial displacements in the load plate such as presented in Figure 14. In this figure, it is also possible to observe that the bolt head and nuts were simulated through UZ displacements restraints at the hole adjacent area.

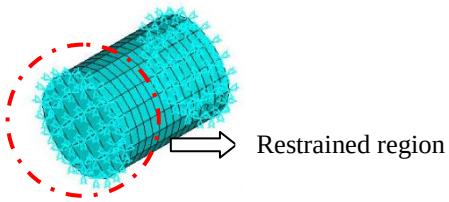

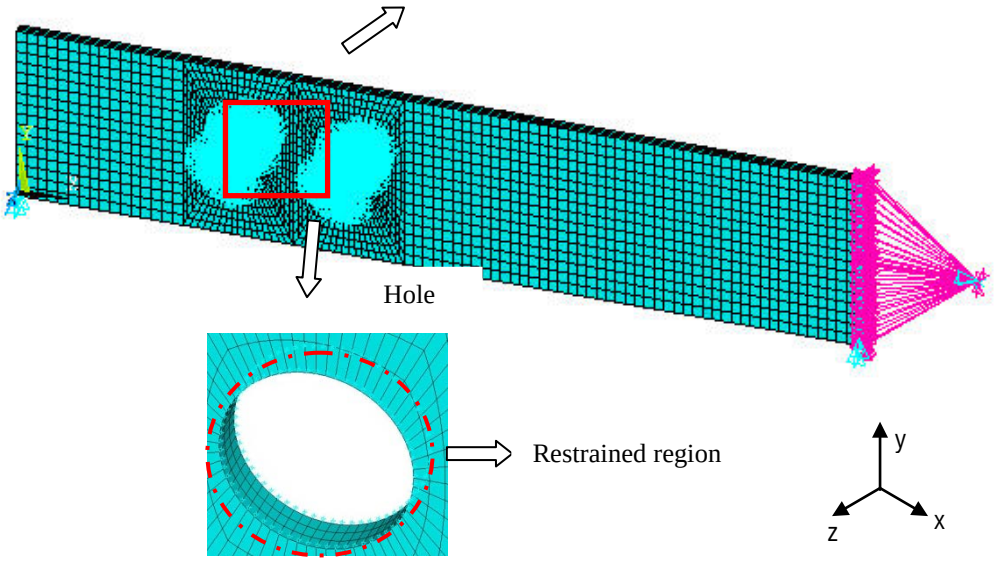

Figure 14 Finite element model and contact elements [12].

The investigation involved the modelling of the experiments made by Santos [11]. Figure 15 presents a typical mesh configuration of the complete model. It is emphasized here that only half of the model was considered using the symmetry boundary conditions being sufficient to characterize the joint ultimate limits states.

The adopted material properties were: Young's modulus of 210 GPa (see Figure 6) and a Poisson's coefficient of 0.3. As previously mentioned, stainless steel true stress *versus* true strain curves with a nonlinear behaviour were adopted using data from the tensile coupons tests Figure 6.

A full nonlinear analysis was performed for the developed numerical model. The material non-linearity was considered using a Von Mises yield criterion associated to a multi-linear stress-strain relationship and isotropic hardening response. The geometrical non-linearity was introduced in the model by using an Updated Lagrangean formulation. This procedure represents the full structural assessment of the analysed bolted joints, and may be summarized in several outputs, namely the stress distribution (that detects, among other data, first yield), or the force-displacement curve for any node within the connection.

Figure 16 presents the load *versus* displacements curves for each individual test, where it can be observed that the ultimate load of experiments E5_INOX_S50, E7_INOX_S30 e E9_INOX_S23 were: 389 kN, 389 kN and 385 kN, respectively. All the numerical model loads were situated in an interval between the experimental loads and the Eurocode 3 (part 1.4 2003) estimated values.

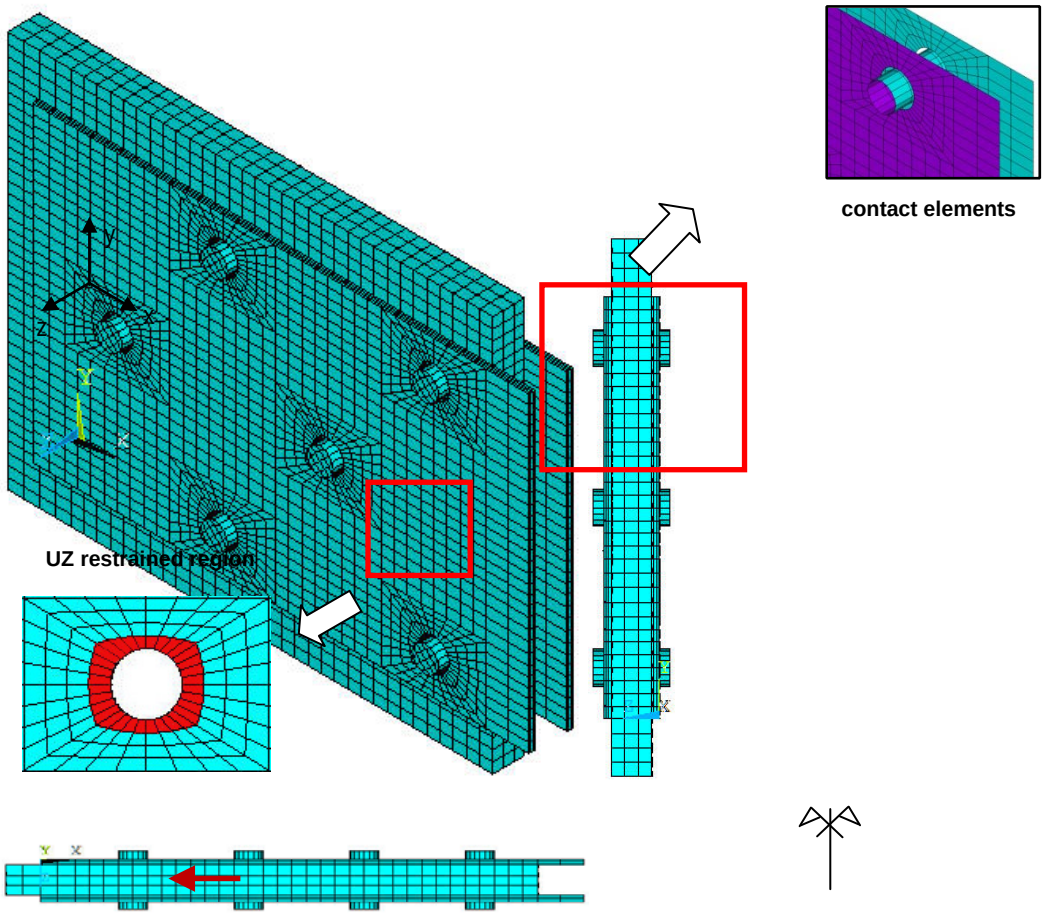

Figure 15 Finite element model and contact elements [12].

Figure 17 depicts the Von Mises stress distributions for the three numerical models, where could be noticed that all models presented high stress concentrations in the region between the bolt holes and the plate edge. In the numerical modelling corresponding to E5_INOX_S50 test the stress distribution indicates a possible rupture in the stainless steel plate net area passing through two bolt holes, mode of failure that also occurred in the experiment. In the numerical modelling corresponding to E7_INOX_S30, the section in which the net area rupture occurs is not clear, i. e. it could be located in the plate region passing through two or three bolt holes. In the numerical modelling corresponding to E9_INOX_S23 test the stress distribution indicates a possible rupture in the stainless steel plate net area passing through three bolt holes, failure mode that also was identified in the experiment.

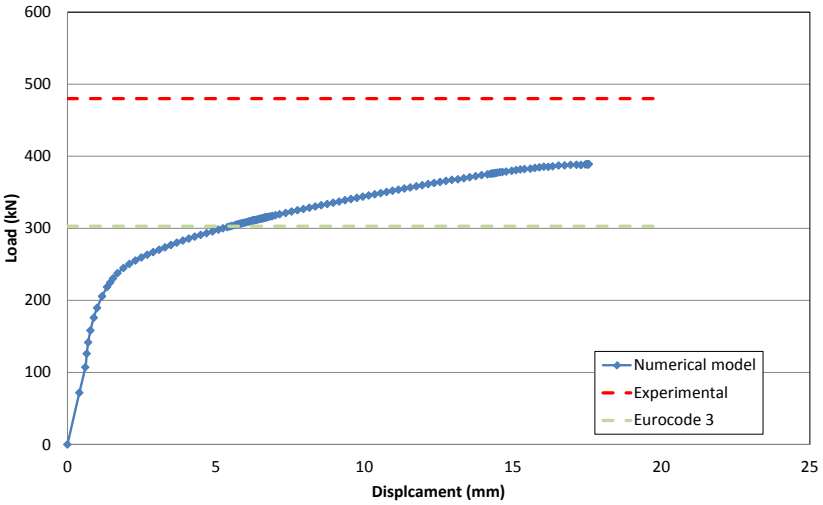

E5_INOX_S50 specimen

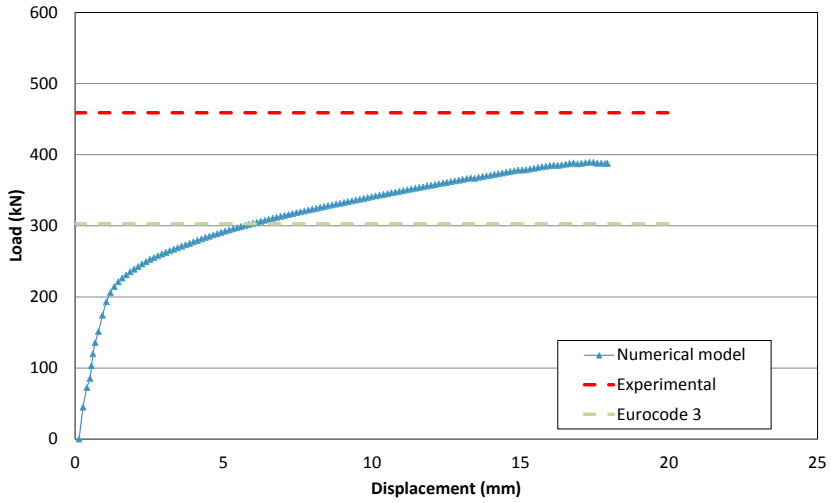

E7_INOX_S30 specimen

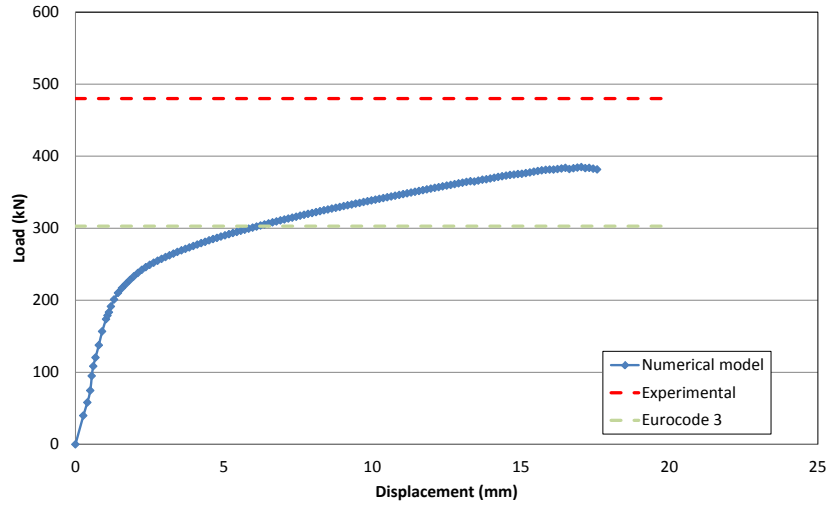

E9_INOX_S23 specimen

Figure 16 Stainless steel load *versus* displacement curves [12].

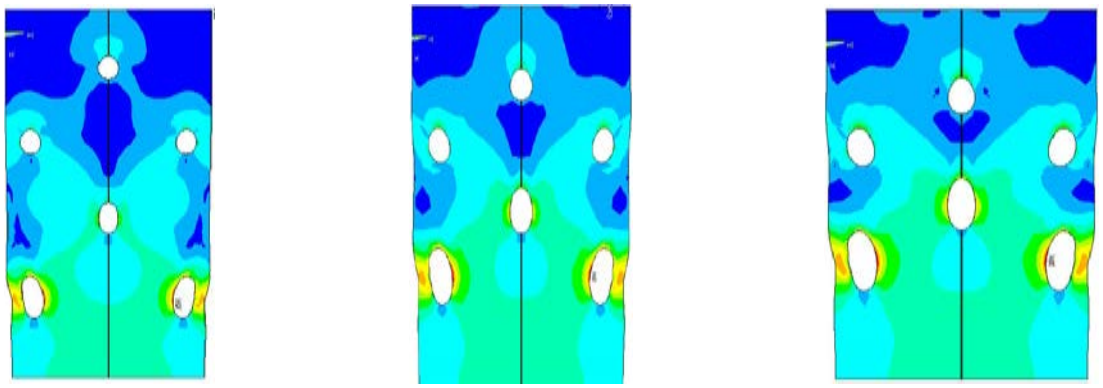

a) Test – E5_INOX_S50 b) Test – E7_INOX_S30 c) Test – E9_INOX_S23

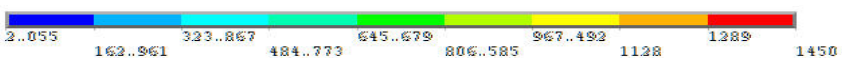

Figure 17 Von Mises stress distribution (in MPa) at the ultimate load.

In order to validate the proposed numerical model, a series of comparisons will be presented in terms of load vs. deflections curves for specific points that were measured in the experimental programme. Figure 18 presents typical numerical and experimental strain comparisons for the E5_INOX_S50 specimen, measured in the region close to the joint centre line and to the symmetry axes. It can be observed that a similar response was found in the numerical and

experimental curves, for strain gauges 2(4) and 3(8). However, the numerical model presented, in the plastic range, a stiffness value lower than their experimental counterparts, for both investigated points. For the E7_INOX_S30 test the numerical model results were not as good as the previous tests, presenting, for all the load levels, a lower stiffness and achieving larger strains than its experimental counterparts. Alternatively, the results of E9_INOX_S23 tests, indicated a good similarity between the numerical and experimental evidences.

The plate section at which the stainless steel net area rupture failure mode occurred was determined with the aid of Figure 19 where load vs. strain curves are illustrated for a point locates at the plate cross section with two bolt holes at the horizontal symmetry axes. From this graph it can be observed that as the horizontal distance between two bolt holes increases the magnitude of the stresses on the bolt present in adjacent section diminishes. For example, for a 250 kN load level, the left curve is associated to a strain level lower than the rest highlighting the net area rupture failure passing in a plate section with three bolt holes. On the other hand, for this load level, E5_INOX_S50 numerical model, highlights that the failure mode is associated to the net area rupture failure passing in a plate section with two bolt holes.

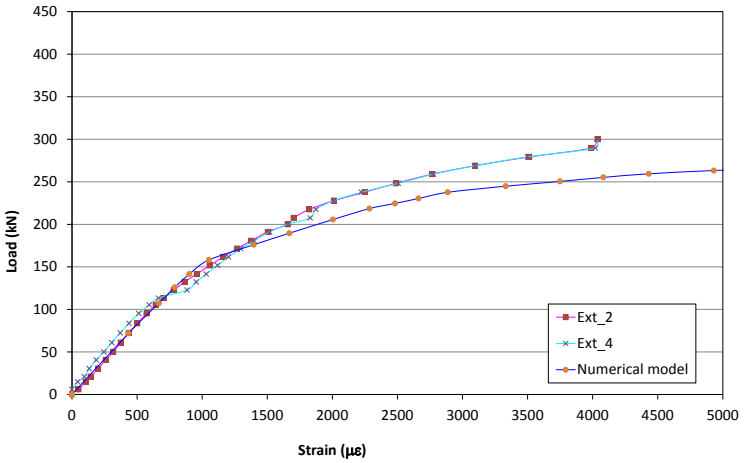

Strain gauges 2 and 4

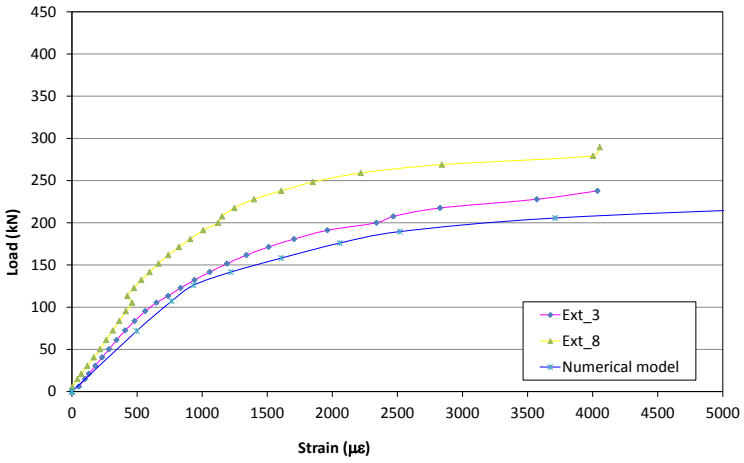

Strain gauges 3 and 8

Figure 18: Load *versus* strain (Experimental *versus* Numerical) - E5_INOX_50 [12].

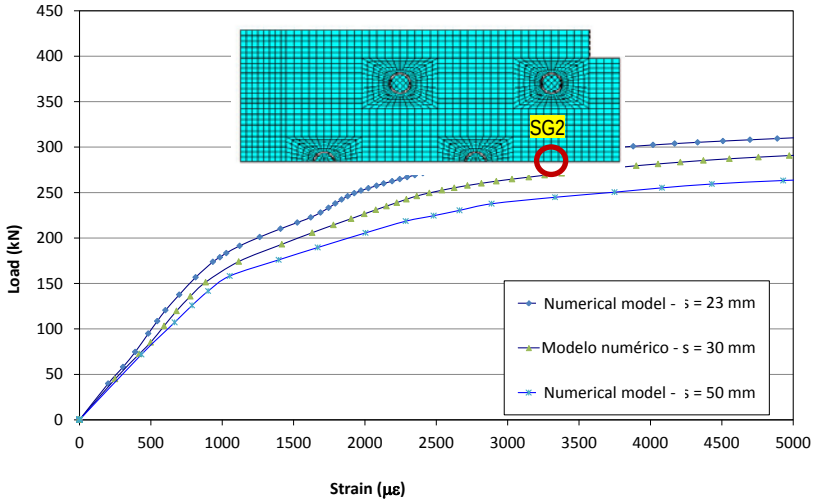

Figure 19 Load *versus* strain curves for all the numerical models [12].

5 Final Considerations

This investigation presented an experimental and numerical programme to investigate the structural response of the carbon steel and stainless steel plates with staggered bolts under tension. Initially the experimental results were compared to theoretical results according to Eurocode 3 provisions [2], [3]. For carbon steel tests, a good agreement was reached between the design equation and the experiments, fact that was not corroborated in the stainless steel tests where large difference were observed, mainly in terms of the ultimate load. A possible explanation for these discrepancies could be related to the fact that the great majority of stainless steel structural design codes is still based on carbon steel analogies.

A finite element numerical model was also developed with the aid of the Ansys 11.0 program and considered material and geometrical nonlinearities through the Von Mises yield criterion and the updated Lagrangian formulation, respectively. Table 6 of Santos [11] presents a comparison between the numerical results and the Eurocode 3 provisions for the already mentioned stainless steel tests. Differences of about 28% were found when the Eurocode 3 [2], [3] and the numerical models were compared.

The numerical ultimate loads were less than their experimental counterparts for all the investigated specimens. This can be explained by the fact that the developed numerical models represent the joints in an idealized form, without imperfections or residual stresses. Another reason for these differences can be attributed to the fact that the stainless steel stress *versus* strain curve adopted in the finite element model was obtained through a series of coupons that are influenced by the rolling direction.

The problem related to the numerical and experimental assessment of stainless and carbon bolted tensioned members is certainly much more complicated and is influenced by several other design parameters. Further research in this area is currently being carried out, in order to consider imperfections, residual stresses and the coupons rolling directions.

On the other hand, differences varying from entre 12% up to 19% were found when the numerical and the experimental values were compared. These differences were also partly due to the natural conservatism present in most of the design standards Eurocode 3, part 1.4 [3]. This conservatism is largely due to the lack of experimental evidence regarding stainless steel structural response still present in the literature.

6 Acknowledgments

The authors would like to thank CAPES, CNPq and FAPERJ for the financial support to this research program. Thanks are also due to ACESITA and USIMINAS for donating the stainless and carbon steel plates used in the experiments.

References

[1] Gardner L, Baddoo N. R., Fire testing and design of stainless steel structures. Journal of Constructional Steel Research; 62: 532-43, 2006.

[2] Eurocode 3, ENV 1993-1-1, 2003: Design of steel structures - Structures – Part 1-1: General rules and rules for buildings. CEN, European Committee for Standardisation, Brussels, 2003.

[3] Eurocode 3, ENV 1993-1-4, 2003: Design of steel structures – Part 1.4: General rules – Supplementary rules for stainless steel, CEN - European Committee for Standardisation 1996.

[4] Burgan B. A, Baddoo, N. R., Gilsenan, K. A., Structural design of stainless steel members - comparison between Eurocode 3, Part 1.4 and test results. Journal of Constructional Steel Research; 54(1):51–73, 2000.

[5] Kouhi J., Talja, A., Salmi, P., Ala-Outinen, T., Current R&D work on the use of stainless steel in construction in Finland. Journal of Constructional Steel Research; 54(1):31–50, 2000.

[6] Van Den Berg, G. J., The effect of the non-linear stress–strain behaviour of stainless steels on member capacity. Journal of Constructional Steel Research;54(1):135–60, 2000.

[7] Gardner, L., Nethercot, D. A., Experiments on stainless steel hollow sections — Part 1: Material and cross-sectional behaviour. Journal of Constructional Steel Research ;60:1291–318.cap 3, 2004.

[8] Salih, E. L., Gardner, L., Nethercot, D. A., Bearing failure in stainless steel bolted connections - Imperial College London, United Kingdom - Engineering Structures 33(2): 549–562, 2011.

[9] Cochrane, V. H., 1922, Rules for Rivet Hole Deduction in Tension Members, Engineering News-Record, vol. 80, November 16.

[10] Kim, T. S., Kuwamura, H., Finite element modeling of bolted connections in thin-walled stainless steel plates under static shear. Thin-Walled Structures, 45(4): 407-421, 2007.

[11] Santos, J. de J. dos, 2008, Comportamento Estrutural de Elementos em Aço Inoxidável, MSc in Civil Engineering, State University of Rio de Janeiro, UERJ, Rio de Janeiro, Brazil (in portuguese).

[12] Silva, A. T. da, 2008, *Comportamento de Peças Tracionadas em Esruturas de Aço-Carbono e Aço Inoxidável*, Graduate Project, Structural Engineering Department, State University of Rio de Janeiro, UERJ, Rio de Janeiro, Brazil (in portuguese).

[13] Bursi, O. and Jaspart, J. P., Calibration of a Finite Element Model for Isolated Bolted End-Plate Steel Connections. *Journal of Constructional Steel Researchers*, 44(3): 225-262, 1997.

[14] Ansys, Inc. Theory Reference (version 11.0), 2008.